Supporting Information

$TiO_2/SrTiO_3/g\text{-}C_3N_4$ ternary heterojunction nanofibers: gradient energy band, cascade charge transfer, enhanced photocatalytic hydrogen evolution, and nitrogen fixation

Ran Tao, Xinghua Li*, Xiaowei Li, Changlu Shao*, Yichun Liu

Centre for Advanced Optoelectronic Functional Materials Research, and Key Laboratory of UV-Emitting Materials and Technology (Northeast Normal University), Ministry of Education Changchun 130024 (P.R. China)

Corresponding Authors

**E-mail: clshao@nenu.edu.cn*

**E-mail: lixh781@nenu.edu.cn*

Tel: +86 43185098803

1. Experimental section

1.1. Characterization

The morphologies of the samples were characterized by the scanning electron microscopy (SEM; Quanta 250FEG) and the high-resolution transmission electron microscopy (HRTEM; JEOL JEM-2100). X-ray diffraction (XRD) patterns were measured using the Rigaku D/MAX-2500 X-ray spectrometer with a CuK line of 0.1541 nm. Fourier Transform infrared spectroscopy (FTIR) spectra were recorded via an Aipha-Centuart FTIR spectrometer (KBr). X-ray photoelectron spectroscopy (XPS) spectra were obtained using the VG-ESCALAB LKII instrument with a Mg Kα ADES ($h\upsilon$ = 1253.6 eV) source at a residual gas pressure of below 10^{-8} Pa. UV-vis absorption spectra were measured by a UV-vis spectrophotometer (UH4150 PerkinElmer Co.), in which $BaSO_4$ was used as the background. Mott-Schottky plots were characterized with a standard three-electrode cell by a Model 660D electrochemical workstation. Thermal gravimetric curves (TG) were carried out via an SDT Q600 thermo-analyzer (TA instruments) from 20 to 900°C at a heating rate of 10°C min^{-1} in air atmosphere. Specific surface areas were measured with a Micromeritics ASAP-2020 instrument and analyzed by the Brunauer-Emmett-Teller (BET) method. Photoluminescence (PL) spectra were collected on a Jobin Yvon HR800 micro-Raman spectrometer using the 325 nm line from a He-Cd laser as an excitation source. Time-resolved transient PL spectra were obtained by Photon Technology International (PTI) TimeMaster™ 400 with pulsed nitrogen lasers as an excitation source.

1.2. Electrochemical measurements

The photocurrent measurements and the electrochemical impedance spectroscopy were measured with a three-electrode electrochemical cell using an electrochemical workstation (CHI 660D, Chenhua Instrument Company, Shanghai, China). FTO glass, platinum net, and Ag/AgCl electrode (saturated KCl) were used as photoelectrode, counter electrode, and reference electrode, respectively. The mixture of 5 mg sample and 100 μL Triton X-100 (1%) was evenly spread on the FTO with an effective area of 1 cm × 1 cm and then heated at 300°C for 1 hour. A 150 W Xe lamp (CHF-XM35, Beijing Chang Tuo) with a light filter (CEL-AM 1.5) was used to as the light source. Before irradiation, the electrolyte solution (0.2 M Na_2SO_4) was degassed by purging with N_2 gas for 20 min. Moreover, the fundamental frequency was 1 kHz, and the scanning voltage range was -1.6 V to +0.4 V vs. Ag/AgCl in Mott-Schottky test.

1.3 The apparent quantum efficiency (AQE) calculation

The AQE of H_2 evolution was calculated by following eq.:

$$AQE = \frac{the\ number\ of\ reactedelectrons}{the\ number\ of\ incidentphotons} \times 100\% \quad (1)$$

$$= \frac{2 \times number\ of\ evolved\ H_2\ molecules}{the\ number\ of\ incident\ photons} \times 100\%$$

$$= \frac{2 \times N_a \times N}{PSt\lambda / hc}$$

where, N_a, N, P, S, t, λ, h, and c stand for Avogadro's constant, the number of moles of generated H_2, optical power density, irradiated area, irradiation time, wavelength of monochromatic light, Planck's constant, and velocity of light, respectively.

The AQE of nitrogen fixation was calculated as following eq.:

$$AQE = \frac{the\ number\ of\ reactedelectrons}{the\ number\ of\ incidentphotons} \times 100\% \quad (2)$$
$$= \frac{3 \times number\ of\ evolved\ ammonia\ molecules}{the\ number\ of\ incident\ photons} \times 100\%$$
$$= \frac{3 \times N_a \times N}{PSt\lambda / hc}$$

where, N_a, N, P, S, t, λ, h, and c stand for Avogadro's constant, the number of moles of generated ammonia, optical power density, irradiated area, irradiation time, wavelength of monochromatic light, Planck's constant, and velocity of light, respectively.

2. Supplementary data

Table S1 H_2 evolution rate of $TiO_2/SrTiO_3/g\text{-}C_3N_4$ nanofibers compared to some previously reported materials.

Samples	Irradiation light	Capturer	H_2 evolution rate ($\mu mol \cdot g^{-1} \cdot h^{-1}$)
This work	300 W Xe lamp AM 1.5	10 vol% methanol	1304
	300 W Xe lamp $\lambda > 400$ nm	10 vol% methanol	504
$g\text{-}C_3N_4/TiO_2$ nanofibers[1]	150 W Xe lamp $\lambda > 400$ nm	10 vol% methanol	252
$Ag/g\text{-}C_3N_4/TiO_2$[2]	300 W Xe lamp AM 1.5	15 vol% TEOA	300
N-doped $TiO_2/g\text{-}C_3N_4$[3]	350 $mW \cdot cm^{-2}$ Xe lamp $\lambda > 420$ nm	20 vol% methanol	296
$g\text{-}C_3N_4/TiO_2$ nanosheets[4]	150 W Xe lamp 200 nm < λ < 2500 nm	10 vol% TEOA	770
$g\text{-}C_3N_4$/ TiO_2(anatase/brookite)[5]	800 W Xe-Hg lamp $\lambda > 420$ nm	20 vol% TEOA	30
$g\text{-}C_3N_4/TiO_2$ composites[6]	500 W Xe lamp $\lambda > 420$ nm	25 vol% methanol	354
$TiO_2/g\text{-}C_3N_4$ composite[7]	450 W mercury lamp	12.5 vol%	75

	λ > 400 nm	methanol	
C-doped TiO_2@g-C_3N_4	300 W Xe lamp	10 vol%	
			36
nanospheres[8]	λ > 420 nm	methanol	
	300 W Xe lamp		
$SrTiO_3$-TiO_2[9]		Overall	212
	UV-Vis		
$SrTiO_3$/TiO_2/H-titanate	300 W Xe lamp	20 vol%	
			26
composite[10]	UV-Vis	methanol	

Table S2 Nitrogen fixation rate of $TiO_2/SrTiO_3/g\text{-}C_3N_4$ nanofibers compared to some previously reported materials.

Samples	Irradiation light	Capturer	Nitrogen fixation rate ($\mu mol \cdot g^{-1} \cdot h^{-1} \cdot L^{-1}$)
This work	300 W Xe lamp AM 1.5	10 vol% methanol	2192
	300 W Xe lamp $\lambda > 400$ nm	10 vol% methanol	891
$g\text{-}C_3N_4/ZnMoCdS$[11]	250 W sodium lamp $\lambda > 400$ nm	0.1 vol% ethanol	194
$g\text{-}C_3N_4/rGO$[12]	250 W sodium lamp $\lambda > 400$ nm	1 mmol L^{-1} EDTA-2Na	515
$g\text{-}C_3N_4/Mg_{1.1}Al_{0.3}Fe_{0.2}O_{1.7}$[13]	250 W sodium lamp $\lambda > 400$ nm	0.1 vol% ethanol	417
$g\text{-}C_3N_4/Zn_{0.11}Sn_{0.12}Cd_{0.88}S_{1.12}$[14]	250 W sodium lamp $\lambda > 400$ nm	0.1 vol% ethanol	419
Cu^+-doped $g\text{-}C_3N_4$[15]	250 W sodium lamp $\lambda > 400$ nm	0.1 vol% ethanol	489
Fe^{3+}-doped $g\text{-}C_3N_4$[16]	250 W sodium lamp $\lambda > 400$ nm	0.1 vol% ethanol	300
$SiW_{12}/K\text{-}C_3N_4$[17]	100 $mW \cdot cm^{-2}$ Xe lamp	-	353

g-C_3N_4-nitrogen vacancies[18]	250 W sodium lamp λ > 400 nm	0.1 vol% ethanol	351
g-C_3N_4-nitrogen vacancies[19]	250 W sodium lamp λ > 400 nm	1 mmol L^{-1} EDTA-2Na	333
g-C_3N_4[20]	250 W sodium lamp λ > 400 nm	0.1 vol% ethanol	167

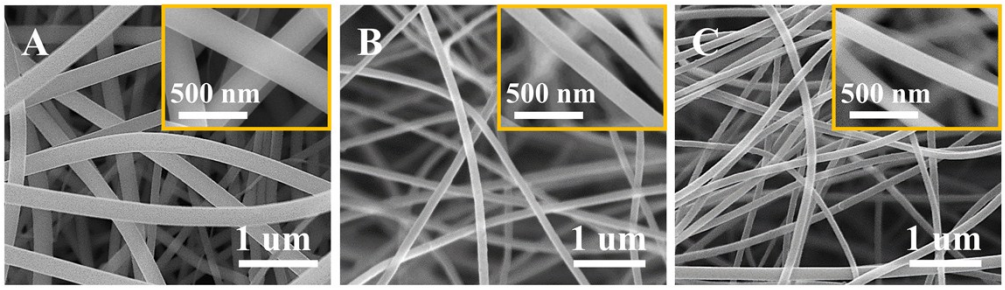

Fig. S1 SEM images of (A) TiO_2, (B) $SrTiO_3$, and (C) $TiO_2/SrTiO_3$ nanofibers at low and high magnification (insets).

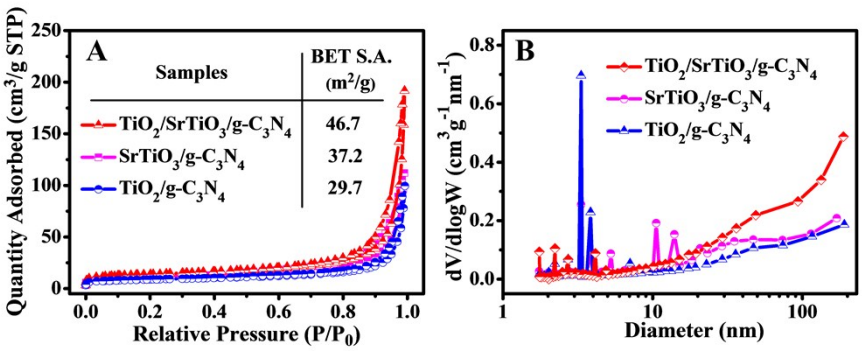

Fig. S2 (A) BET nitrogen adsorption-desorption isotherms and (B) pore-size distribution of TiO_2/g-C_3N_4, $SrTiO_3$/g-C_3N_4, and TiO_2/$SrTiO_3$/g-C_3N_4 nanofibers.

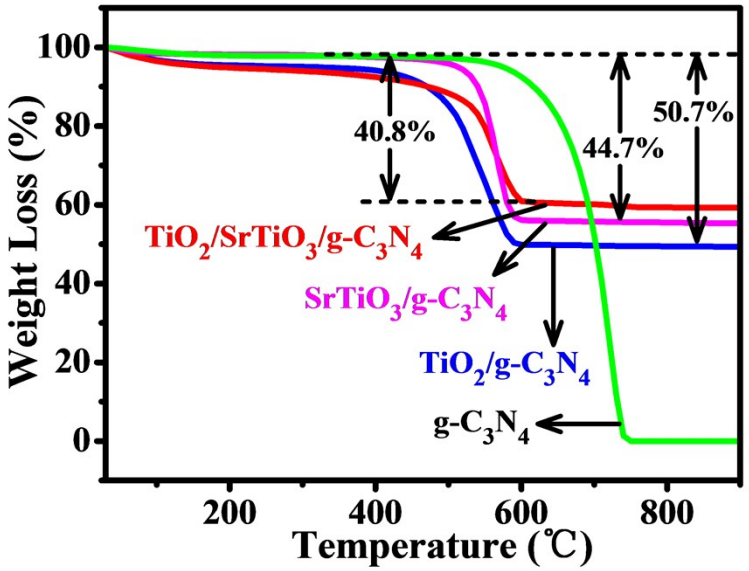

Fig. S3 TG curves of pure g-C_3N_4 powders, TiO_2/g-C_3N_4, $SrTiO_3$/g-C_3N_4, and TiO_2/$SrTiO_3$/g-C_3N_4 nanofibers.

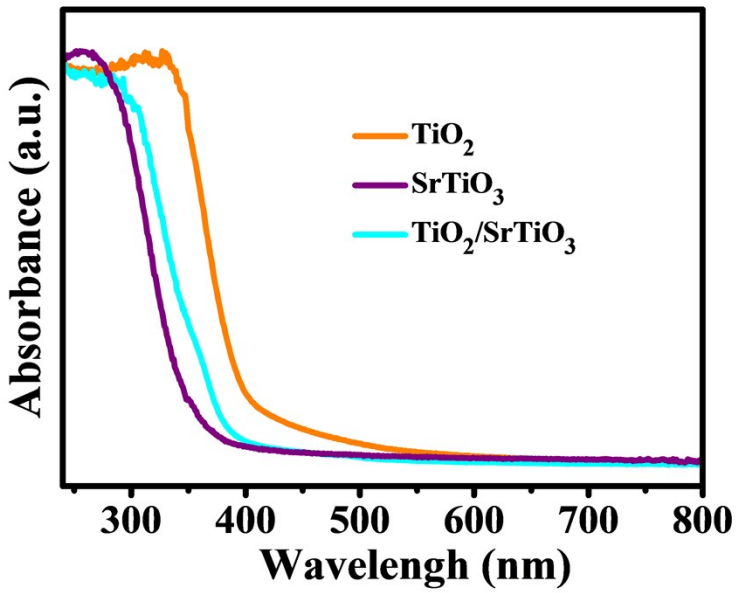

Fig. S4 UV-vis absorption spectra of TiO_2, $SrTiO_3$, and $TiO_2/SrTiO_3$ nanofibers.

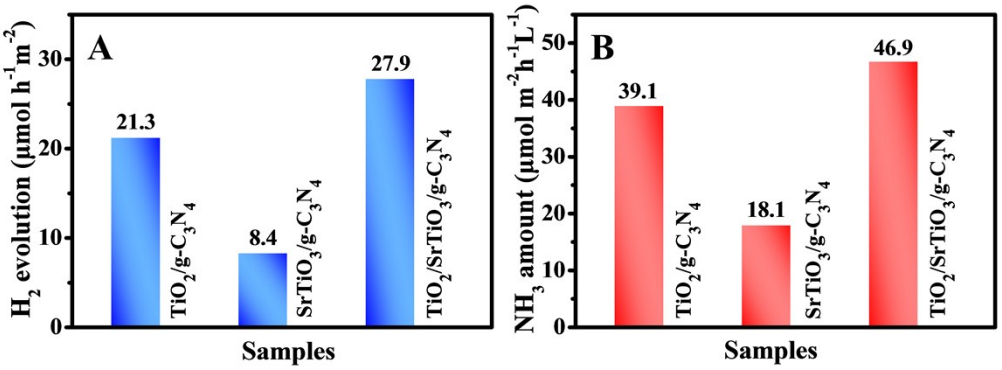

Fig. S5 The photocatalytic (A) H_2 evolution and (B) nitrogen fixation efficiency of TiO_2/g-C_3N_4, $SrTiO_3$/g-C_3N_4, and TiO_2/$SrTiO_3$/g-C_3N_4 nanofibers.

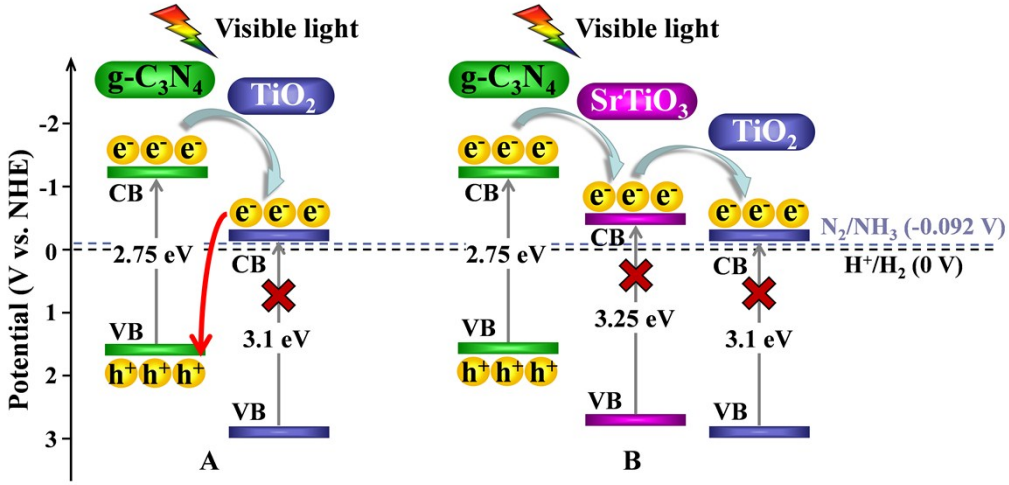

Fig. S6 The photocatalytic mechanism of (A) TiO_2/g-C_3N_4 and (B) TiO_2/$SrTiO_3$/g-C_3N_4 heterojunctions under visible light irradiation.

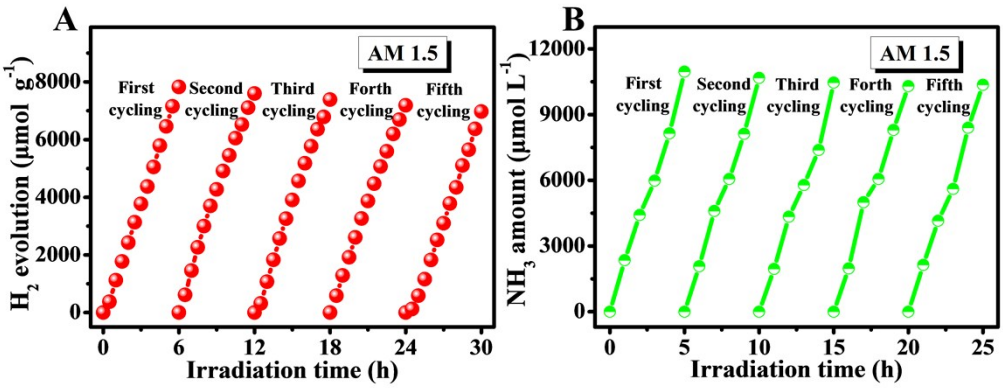

Fig. S7 Cycling tests for five times of photocatalytic (A) H_2 evolution and (B) nitrogen fixation over $TiO_2/SrTiO_3/g\text{-}C_3N_4$ nanofibers under simulated sunlight.

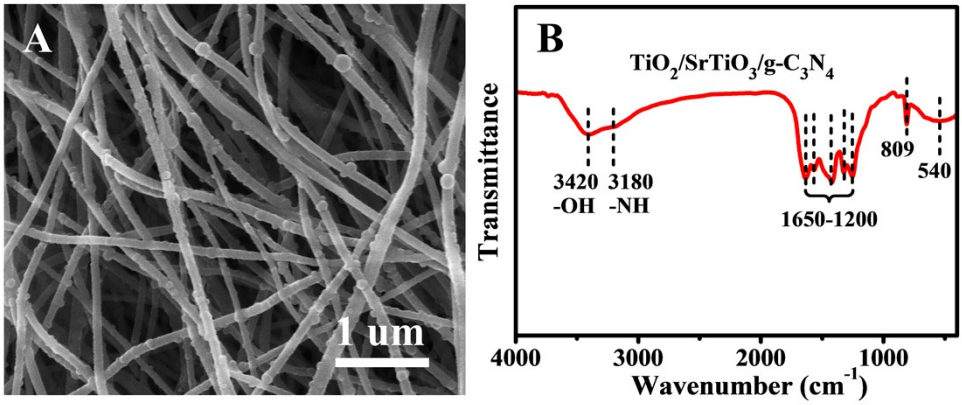

Fig. S8 (A) SEM image and (B) FTIR spectrum of $TiO_2/SrTiO_3/g\text{-}C_3N_4$ nanofibers after photocatalytic H_2 evolution reaction.

References

1. X. Zhou, C. Shao, X. Li, X. Wang, X. Guo and Y. Liu, *J. Hazard. Mater.*, 2018, **344**, 113-122.
2. X. Wei, C. Shao, X. Li, N. Lu, K. Wang, Z. Zhang and Y. Liu, *Nanoscale*, 2016, **8**, 11034-11043.
3. X. W. Shi, M. Fujitsuka, Z. Z. Lou, P. Zhang and T. Majima, *J. Mater. Chem. A,* 2017, **5**, 9671–9681.
4. J. Yan, H. Wu, H. Chen, Y. Zhang, F. Zhang and S. F. Liu, *Appl. Catal. B Environ.*, 2016, **191**, 130-137.
5. Q. Tay, X. Wang, X. Zhao, J. Hong, Q. Zhang, R. Xu and Z. Chen, *J. Catal.*, 2016, **342**, 55-62.
6. A. Qu, X. Xu, H. Xie, Y. Zhang, Y. Li and J. Wang, *Mater. Res. Bull.*, 2016, **80**, 167-176.
7. H. Yan and H. Yang, *J. Alloy. Compd.*, 2011, **509**, L26-L29.
8. Y. Zou, J.-W. Shi, D. Ma, Z. Fan, L. Lu and C. Niu, *Chem. Eng. J.*, 2017, **322**, 435-444.
9. Y. Wei, J. Wang, R. Yu, J. Wan and D. Wang, *Angew. Chem. Int. Ed.*, 2019, **58**, 1422-1426.
10. Y. X. Liu, Z. L. Wang, W. D. Wang, X. Q. An, S. Y. Mi, J. W. Tang and W. X. Huang, *Appl. Sci. Surf.*, 2014, **315**, 314-322.
11. Q. Zhang, S. Hu, Z. Fan, D. Liu, Y. Zhao, H. Ma and F. Li, *Dalton T.*, 2016, **45**, 3497-3505.
12. S. Hu, W. Zhang, J. Bai, G. Lu, L. Zhang and G. Wu, *RSC Adv.*, 2016, **6**, 25695-25702.
13. Y. Wang, W. Wei, M. Li, S. Hu, J. Zhang and R. Feng, *RSC Adv.*, 2017, **7**, 18099-18107.
14. S. Hu, Y. Li, F. Li, Z. Fan, H. Ma, W. Li and X. Kang, *ACS Sustain. Chem. Eng.*, 2016, **4**, 2269-2278.
15. S. Hu, X. Qu, J. Bai, P. Li, Q. Li, F. Wang and L. Song, *ACS Sustain. Chem. Eng.*, 2017, **5**, 6863-6872.
16. S. Hu, X. Chen, Q. Li, F. Li, Z. Fan, H. Wang, Y. Wang, B. Zheng and G. Wu, *Appl. Catal. B Environ.*, 2017, **201**, 58-69.
17. C. Xiao, L. Zhang, K. Wang, H. Wang, Y. Zhou and W. Wang, *Appl. Catal. B Environ.*, 2018, **239**, 260-267.
18. H. Ma, Z. Shi, Q. Li and S. Li, *J. Phys. Chem. Solids*, 2016, **99**, 51-58.
19. G. Wu, Y. Gao and B. Zheng, *Ceram. Int.*, 2016, **42**, 6985-6992.
20. H. Ma, Z. Shi, S. Li and N. Liu, *Appl. Surf. Sci.*, 2016, **379**, 309-315.